Hakimhashemi, A., Schoenball, M., Heidbach, O., Zang, A., Grünthal, G. (2014): Forward modelling of seismicity rate changes in georeservoirs with a hybrid geomechanical–statistical prototype model. - *Geothermics*, *52*, p. 185-194.

DOI: http://doi.org/10.1016/j.geothermics.2014.01.001

Geothermics 52 (2014) 185-194

# Forward modelling of seismicity rate changes in georeservoirs with a hybrid geomechanical-statistical prototype model

Amir Hossein Hakimhashemi[a,*], Martin Schoenball[b], Oliver Heidbach[a], Arno Zang[a], Gottfried Grünthal[a]

[a] *Helmholtz Centre Potsdam, GFZ German Research Centre for Geosciences, Potsdam, Germany*
[b] *Karlsruhe Institute of Technology (KIT), Karlsruhe, Germany*

A R T I C L E I N F O

*Article history:*
Received 17 October 2012
Received in revised form 7 November 2013
Accepted 8 January 2014
Available online 25 January 2014

*Keywords:*
Geomechanical-statistical model
Georeservoir
Induced seismicity
Seismicity rate

A B S T R A C T

A key challenge for the development of Enhanced Geothermal Systems (EGS) is to forecast the probability of occurrence of seismic events that have the potential to damage man-made structures. Induced seismicity results from man-made time-dependent stress changes, e.g., due to fluid injection, shut-in and fluid or steam production. To accomplish a classical Probabilistic Seismic Hazard Assessment (PSHA) a catalogue of induced seismicity is required. In addition, PSHA does not return any practical recommendation for how to treat the reservoir geomechanically in order to lower the probability of occurrence of induced seismicity. Thus, we propose to link the simulated stress changes from forward geomechanical numerical reservoir models with the statistical rate-and-state approach of *Dieterich* (1994). Using this link we translate the modelled time-dependent stress changes into time-dependent changes of seismicity rates. This approach is general and independent of the incorporated geomechanical numerical model used. We exemplify our hybrid model approach using a geomechanical model that describes the stimulation of the well GPK4 at the EGS site in Soultz-sous-Forêts (France) including the shut-in phase. By changing the injection rate in the geomechanical model we generate various synthetic injection scenarios. With these scenarios we can study the effect on the seismicity rate and provide a recommendation for which injection experiment results in the least increase of seismicity rate. The results indicate an explicit coupling between the time-depending stress changes and the induced seismicity rate for each scenario. Even though the hybrid model cannot be used in general to derive absolute values of the rate of induced seismicity a priori (this is only possible if the geomechanical model can be calibrated against observed induced events), it serves as a tool to test the effect of stress changes on the induced seismicity rate. The approach described here is a prototype model illustrating the general workflow. In particular the geomechanical model can be replaced by any other type of reservoir description.

## 1. Introduction

Enhanced geothermal systems (EGS) have the potential to be major pillars in the future mix of renewable energy supply (*Tester et al.*, 2006). However, in the past decade a number of larger induced seismic events, which had the potential to damage the man-made structures, raised major concern amongst the public and the political decision makers (*Evans et al.*, 2012; *Majer et al.*, 2007, 2012). Induced seismicity is not restricted to EGS sites, but occurs also in hydrocarbon reservoirs due to gas and oil depletion, re-injection of fluids to maintain or enhance the reservoir pressure or potash and coal mining to name a few (*Grünthal*, 2013; *Suckale*, 2009, 2010).

In Europe in particular the two induced events at the geothermal sites in Basel (Switzerland) and Landau i.d. Pfalz (West Germany in the Upper Rhine Graben) resulted in an ongoing discussion on safety aspects of geothermal sites in general. In Basel an $M_L = 3.4$ event was induced on December 8th 2006 shortly after the shut-in of a four day stimulation experiment (*Deichmann and Ernst*, 2009; *Deichmann and Giardini*, 2009; *Häring et al.*, 2008). In Landau an $M_w = 2.6$ induced event occurred on August 15th 2009 after an instant shut-in within the production phase of the geothermal plant (*Grünthal*, 2013). As a result the project at Basel has been abandoned and the power plant in Landau is running in testing phase with reduced injection pressure.

Thus a key challenge for EGS sites is to forecast the probability of occurrence of induced seismicity that can potentially produce damage to structures at the surface and to develop strategies for reservoir treatment that lower the probability of occurrence of such induced seismicity. In general, for the case of tectonic earthquakes, a classical Probabilistic Seismic Hazard Assessment (PSHA) can be applied (*Cornell*, 1968; *Grünthal & Wahlström*, 2006; *McGuire*, 2004). A classical PSHA determines the frequency, i.e. the number of events per unit of time, with which a property of an earthquake that can cause damage will occur (*McGuire*, 2004). However, to accomplish a classical PSHA a catalogue of seismic events is required (in this context, particularly, a catalogue of induced seismic events, or a synthetic earthquake catalogue from numerical experiments). Although the tectonic earthquakes can be used to calculate the natural background seismic hazard at a specific EGS site, the information gained from the tectonic earthquakes is inappropriate to be applied to calculate the seismic

* Corresponding author. Tel.: +49 331 288 1264; fax: +49 331 288 1127.
*E-mail address:* hakim@gfz-potsdam.de (A. Hossein Hakimhashemi)

hazard associated with the induced seismicity in the EGS sites concerning different phases; i.e., stimulation phases and production phases. Furthermore, no practical guideline can be expected from classical PSHA addressing how to mitigate the probability of occurrence of induced seismicity.

So far, several approaches have been proposed and tested to handle the probability of occurrence of induced seismicity during stimulation and the shut-in phase. For the traffic light system introduced by *Bommer et al.* (2006) seismicity is recorded instrumentally in real-time. Macroseismic observations reported from the public are also taken into account. Once the recorded peak ground velocity is above a given threshold the stimulation has to be stopped. However, the system failed in Basel. The injection experiment was stopped when an event of $M_L = 2.6$ was recorded. Nevertheless, the $M_L = 3.4$ seismic event occurred shortly after the shut-in (*Deichmann and Giardini*, 2009; *Häring et al.*, 2008). An alternative model that characterizes the seismic response of a reservoir is proposed by *Shapiro et al.* (2010) and *Dinske and Shapiro* (2013). They use the recorded induced seismicity from the injection phase to estimate the potential of the site to produce a certain magnitude–frequency distribution. However, as the pressure source is assumed to be constant or increasing in pressure, the application is limited and cannot be applied to the shut-in phase or in cyclic stimulation experiments. *Barth et al.* (2013) propose a statistical model to assess the change in probability of the occurrence of a damaging event after the shut-in. These and other models have in common that they are all based on the catalogue of induced seismicity. Furthermore, they do not provide a practical answer for how to treat the reservoir hydraulically or means to plan the treatment a priori; i.e., before any man-made changes of the in situ stress state are induced.

A step towards a link between geomechanical numerical reservoir models and tectonic earthquakes is shown by *Passarelli et al.* (2013). They present an approach for how to estimate the probability of whether a tectonic earthquake was triggered by a stress change of a dike intrusion or not. They link a time-independent instantaneous stress change simulated with a displacement in an elastic half-space model, with the rate-and-state (RaS) law of *Dieterich* (1994) and derive which scenario is the most probable to trigger the observed seismicity. They claim that their approach can be used in principal also for man-made induced seismicity in georeservoirs, but their formal approach is limited to time-independent single stress changes. Thus, this is not appropriate for a georeservoir where stress changes are in general strongly time-dependent during fluid injection experiments and after shut-in.

Thus, two fundamental requests are yet not fulfilled for a practical usage of models before the reservoir is treated by means of stimulation, production or circulation tests: (1) The model should be capable of forecasting the probability of occurrence of damaging induced events and must not rely on a catalogue of induced seismicity. (2) The statistical model should be capable of handling time-dependent stress changes and translate these into seismicity rate changes. The latter is needed as state-of-the-art geomechanical numerical reservoir models include a number of time-dependent processes such as pore pressure diffusion (linear and non-linear) coupled to the elastic response (*Kohl and Mégel*, 2007; *McClure and Horne*, 2011), the so-called pore pressure stress coupling process (*Altmann et al.*, 2010; *Ghassemi and Zhou*, 2011; *Hillis*, 2000), thermal diffusion and combination of these processes on different time-scales for long-term production, stimulation and shut-in and re-injection of waste water (*Baisch et al.*, 2010; *Bruel*, 2007; *Rutqvist et al.*, 2007; *Schoenball et al.*, 2010). Regardless of the complexity of the geomechanical-numerical reservoir model, the output is always at least a change of effective stress, both as a function of time and space. Deriving a synthetic catalogue of induced seismicity from these models is only possible by making further assumptions on the criticality

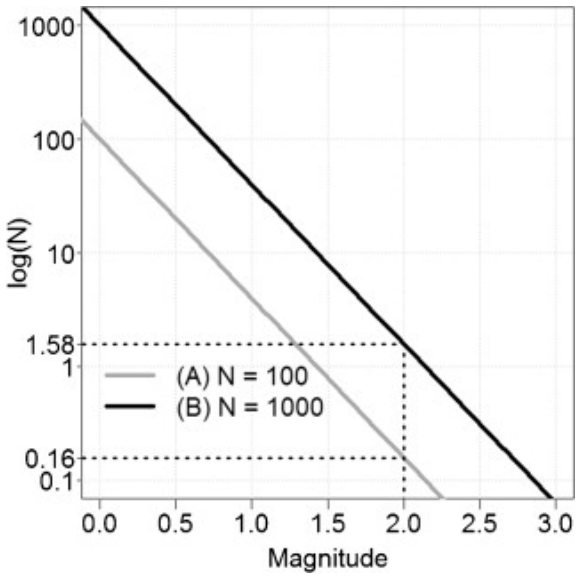


**Figure 1.** Seismicity rate versus magnitude. Assuming that the seismicity rate $N$ is 10 times smaller (grey line) in case A with respect to case B where $N = 1000$ events that occur within a given time span $dt$, the occurrence rate of a magnitude 2.0 event is lowered from a factor of 1.58 in the time span to 0.16.

of the reservoir, the failure criterion and the characteristics of the fracture network that determine the length of failure; i.e., the magnitude of the events (*Bruel*, 2007). In particular the a priori assumption on the distribution of the fracture network (length and density) and its initial stress field (e.g., criticality of the stress state) controls the frequency-magnitude $b$-value and the seismicity rate. The rupture process of a seismic event itself is typically not part of the forward modelling applied to the reservoir scale. So far, the actual rupture process has only been simulated for rock specimens (*Yoon et al.*, 2012), borehole breakouts (*Shen et al.*, 2013), and 2D reservoir models (*Yoon et al.*, 2013). To model the rupture process in 3D is still a challenge.

In this paper we propose a method to translate time-dependent stress changes into time-dependent changes of seismicity rate. The latter is a direct expression of the probability of occurrence of a seismic event in a given time span of a given magnitude class. A lower seismicity rate lowers the probability of occurrence of a given magnitude in a given time span (Fig. 1). This holds, of course, when the slope of the frequency–magnitude curve does not change. We propose here a prototype hybrid model that is capable to link the time-dependent stress changes from any forward geomechanical–numerical reservoir model with the statistical RaS model from *Dieterich* (1994). With this combination it is possible to forecast the seismicity rate and its changes with different reservoir treatments during stimulation and production phases.

To test our prototype hybrid model we use the geomechanical numerical model of *Kohl and Mégel* (2007) that simulates the time-dependent stress changes during the stimulation experiment and after shut-in at the EGS site GPK4 in Soultz-sous-Forêts. We then vary the injection rate of the model to study which treatment results in a lower probability of occurrence of induced seismicity.

In the following section, we describe the geomechanical numerical reservoir model and the processes that are captured by it. Then, we introduce the statistical RaS model and show how we link this to the output of the geomechanical reservoir model. Subsequently, we briefly introduce the EGS site at Soultz-sous-Forêts, France, and the GPK4 stimulation experiment. Finally, in Section 5, the advantage of the hybrid model is presented. Here we perform a variety of different

**Table 1**
Key input parameters of the geomechanical numerical model.

| Parameter | Value |
|---|---|
| Initial matrix permeability | $5 \times 10^{-17}$ m$^2$ |
| Azimuth of $S_{H,max}$ | 170° |
| Friction angle | 34° |
| Dilation angle | 3° |
| *Effective stresses [MPa]* | |
| Maximum horizontal | $51.6 + 0.0110 \cdot (z - 4750\ \text{m})$ |
| Minimum horizontal | $23.8 + 0.0059 \cdot (z - 4750\ \text{m})$ |
| Vertical | $70.2 + 0.0155 \cdot (z - 4750\ \text{m})$ |

injection scenarios to study their impact on the rate of induced seismic events.

## 2. Geomechanical numerical model

The workflow we introduce in this paper is principally applicable to any kind of geomechanical model delivering time-dependent changes of stress and which is suitable to describe the relevant processes in a georeservoir. We exemplify our workflow using the finite element code FRACTure (*Kohl et al.*, 1995), coupled to a 3D stochastic fracture network driven by the code HEX-S to incorporate the fracture mechanical behaviour (*Kohl and Mégel*, 2007). It has been used to successfully forecast the hydraulic response of the reservoir to stimulation of the well GPK4 at Soultz-sous-Forêts. A good match of the non-linear hydraulic response was achieved, and the spatio-temporal characteristics of the seismic response could be forecasted. However, the model is not capable of estimating seismic hazard for a given stimulation treatment; i.e., it cannot forecast event magnitudes. Detailed descriptions of the code and the model of the Soultz reservoir, which are used in this study, are given in *Kohl and Mégel* (2007). Its main features are summarized below.

The model consists of a finite element mesh (Fig. 2) that derives its hydraulic properties from a mapped fracture network. The fracture network is a combination of deterministic fractures and stochastic fractures. Deterministic fractures are obtained from features visible on imaging and flow logs of the wells. Away from the boreholes, the fracture network is complemented by stochastic fractures which are randomly placed in the model volume and given orientation and hydraulic properties representative of the fracture families obtained from borehole logs. Fracture lengths obey a power law distribution with a scaling exponent of one. All fractures, deterministic and stochastic, are then subdivided into individual slip patches, which are considered as separate in subsequent computations. We refer to *Kohl and Mégel* (2007) for a detailed description of the fracture network generation.

The aperture of each slip patch is updated during each time step according to constitutive relations for the fracture-mechanical behaviour following *Willis-Richards et al.* (1996). The aperture responds elastically to changes of pore pressure below a threshold given by the Mohr-Coulomb criterion and is determined by the assumed stress field and the friction angle (Table 1). In the effective stress formulation we use, the minimum critical pore pressure $p_c$ (MPa) that leads to rupture of optimally oriented fractures with $p_c = 5.5 + 0.0021 \cdot (z - 4750$ m) with $z$ as depth in metres. If this threshold is surpassed the Mohr-Coulomb criterion is met and the fracture is subjected to shear, increasing aperture by a dilation angle. This aperture increase is irreversible and considered the enhancement of fracture permeability by the stimulation. The fracture network is then mapped onto the finite element mesh; fracture apertures are transformed to tensorial permeability for each finite element. The next time step of hydraulic calculation is then carried out and the pore fluid pressure field is updated. In order to keep the demonstration of our workflow for hybrid modelling simple, we neglect any second-order couplings such as poroelasticity, thermoelasticity, chemical processes or stress transfer (Table 2).

**Table 2**
Key input parameters of the statistical RaS model.

| Parameter | Value |
|---|---|
| Background shear stressing rate | $10^{-7}$ bar |
| Background seismicity rate | $10^{-7}$ |
| Number of integration points | 1000 |
| $A_\sigma$ | 1-10 bar |

## 3. Time-dependent rate-and-state model and link to the geomechanical numerical model

To translate stress changes; i.e., pore pressure changes, from the numerical geomechanical model into temporal changes of seismicity rate the RaS model by *Dieterich* (1994) is used. The RaS is a general approach to estimate the changes in the seismicity rate caused by some stressing history on faults with rate- and state-dependent friction. In a general RaS model, seismic events nucleation is assumed to occur over a restricted area called the nucleation source. The objective of the RaS approach is to find the time at which each nucleation source initiates a seismic event when subjected to a stressing history (*Dieterich*, 1994).

The RaS model has already been successfully applied to different sequences of seismicity; e.g., aftershock sequences after a large main shock and swarms (*Catalli et al.*, 2008; *Daniel et al.*, 2011; *Dieterich et al.*, 2000; *Toda and Stein*, 2003; *Toda et al.*, 2002). So far, the RaS model by *Dieterich* (1994) has not been applied to calculate the effect of the stress changes, caused by reservoir activities, on the seismicity rate.

In terms of the RaS model, the seismicity rate $R_n(x)$ at time step $n$ at integration point $x$ ($x$ is a location of a potential fracture) in the reservoir is given by

$$R_n(x) = \frac{r(x)}{\gamma_n(x)\dot{\tau}_r} \tag{1}$$

where $r(x)$ is the background seismicity rate at integration point $x$, $\dot{\tau}_r$ is the background stressing rate, and $\gamma_n(x)$ is the state variable at time step $n$ in integration point $x$ obtained by

$$\gamma_n(x) = \left(\gamma_{n-1}(x) - \frac{1}{\dot{\tau}_n(x)}\right)\exp\left(\frac{-(t_n - t_{n-1})\dot{\tau}_n(x)}{A_\sigma}\right) + \frac{1}{\dot{\tau}_n(x)}, \quad \text{for } \dot{\tau}_n(x) \neq 0, \tag{2}$$

where $t_n$ is the total time at time step $n$ and $\dot{\tau}_n(x)$ is the change of the stressing rate during time step $n$. $\gamma_{n-1}(x)$ is the state variable corresponding to the previous time step with $\gamma_0(x) = (1/\dot{\tau}_r)$ for the initial condition of steady state. $A_\sigma$ is the key free parameter comprised of the a priori unknown constitutive fault parameter $A$ and the normal stress $\sigma$ on the fault. $A$ is an experimentally determined coefficient, which includes the effects of all unknown characteristics of the given fault (*Dieterich*, 1994). Parameter $A_\sigma$ is considered as constant and the same for all integration points throughout this paper. For $\dot{\tau}_n(x) \to 0$ Eq. (2) yields to

$$\lim_{\dot{\tau}_n(x)\to 0} \gamma_n(x) = \gamma_{n-1}(x) - \frac{t_n - t_{n-1}}{A_\sigma}. \tag{3}$$

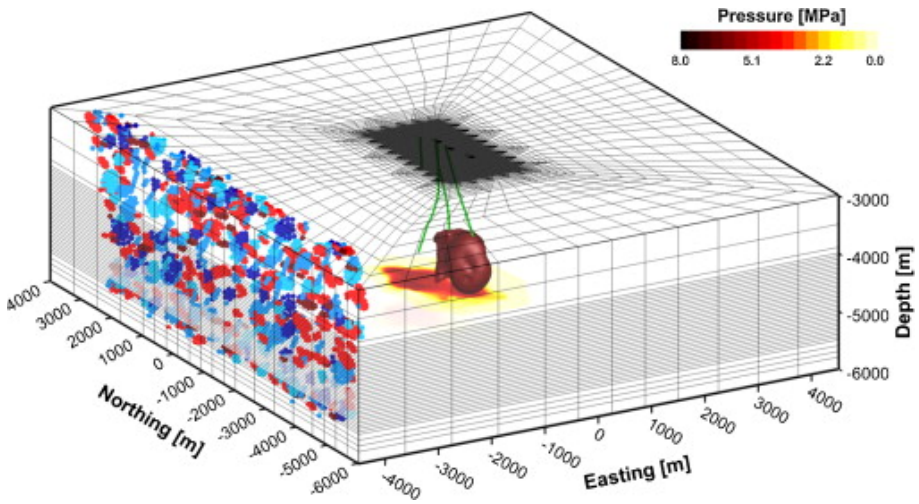


**Figure 2.** 3D finite element mesh of the geomechanical model with Soultz borehole trajectories (green) and modelled pressure distribution (yellow–red). At the left, only a section of the discrete fracture network is shown to provide an impression of fracture distribution and density. For the simulation runs the discrete fracture network is evenly distributed in the whole modelling domain. (For interpretation of the references to color in this figure legend, the reader is referred to the web version of the article.)

It should be mentioned that Eqs. (1)–(3) are appropriate to calculate the seismicity rate in case of gradual changes of stress; e.g., as the effect of fluid injection in a reservoir (*Toda et al.*, 2002). This is different from the original RaS type model concerning a sudden change in stress caused by a large earthquake (*Catalli et al.*, 2008; *Dieterich et al.*, 2000; *Toda and Stein*, 2003) or an instantaneous dyke intrusion as assumed by *Passarelli et al.* (2013). In both cases, a seismicity dataset is required since the stress changes are calculated based on the focal mechanism of an earthquake. This means earthquakes are considered as the sources of a single and instantaneous stress change. *Toda et al.* (2002) and *Daniel et al.* (2011) use a piecewise constant shear stressing rate as the source of changes of stress. Using these stress changes, the RaS model is applied to estimate the upcoming seismicity rate.

In contrast, in our forward RaS model, the seismicity rate is estimated using the stress changes obtained directly from the geomechanical model. To apply the RaS model to the stress changes in each integration point of the reservoir, the pore pressure changes obtained from the geomechanical model in each integration point in the reservoir are transformed to Coulomb stress change by

$$\Delta CFS_n(x) = \Delta\sigma_S(x) - \mu\big(\Delta\sigma_N(x) - \Delta p_n(x)\big), \tag{4}$$

where $\Delta CFS_n(x)$ is the change in Coulomb failure stress in each integration point for time $t_n$. $\Delta\sigma_S(x)$ and $\Delta\sigma_N(x)$ are the shear and normal stress changes in integration point $x$ respectively, and are considered as arbitrary constants during the process. $\Delta p_n(x)$ is the change in calculated pore pressure at time $t_n$ in integration point $x$, and $\mu$ is the friction coefficient considered as constant and has the same value for all integration points in the reservoir. $\dot{\tau}_n(x)$ in Eq. (2) will be then replaced by

$$\dot{\tau}_n(x) = \frac{\Delta CFS_n(x)}{t_n - t_{n-1}} = \frac{\mu\Delta p_n(x)}{t_n - t_{n-1}} \tag{5}$$

Since $\Delta\sigma_S(x)$ and $\Delta\sigma_N(x)$ remain constant during the stimulation process, they are neglected in the calculation of $\dot{\tau}_n(x)$ and consequently in the estimation of the seismicity rate. This means that $\dot{\tau}_n(x)$ is calculated only relative to the changes in pore pressure; i.e., $\Delta p_n(x)$. The seismicity rate of the whole reservoir for each time step $n$ will be then calculated by $R_n = \sum_{x\in X} R_n(x)$, where $X$ is the set of all integration points $x$ in the reservoir. The cumulative seismicity rate from time $t_0$ (when the injection starts, here $t_0 = 0$) until a given time $T$ can then be calculated by

$$\Re(t_0, T) = \int_{t_0}^{T} R(t)dt \approx \sum_{\{n|t_n\le T\}} \frac{(R_n - R_{n-1})(t_n - t_{n-1})}{2}. \tag{6}$$

## 4. Application to the model of GPK4 stimulation at Soultz-sous-Forêts

Our hybrid approach is applied to the model of the stimulation of the well GPK4 at the EGS pilot site in Soultz-sous-Forêts, France. The first stimulation of the well GPK4 was done during a period of about four days in September 2004. The injection was performed at a constant flow rate of 30 L $s^{-1}$, except during three short hydraulic shocks with a flow of about 45 L $s^{-1}$ and one fluid impulse of 60 L $s^{-1}$ (*Dorbath et al.*, 2009). Shut-in was performed with a step at 15 L $s^{-1}$ maintained for about three hours to test soft shut-in. The pressure measured at the GPK4 wellhead (Fig. 3a) reached a constant value of around 170 bar quite fast (*Dorbath et al.*, 2009). During the short episodes of increased pumping at 45 L $s^{-1}$ only slight increases of pressure of around 10 bar were measured, which shows the highly non-linear response of the fractured reservoir to increments of flow rate (*Kohl et al.*, 1997).

In the geomechanical model the flow rate was used as Neumann boundary condition, the corresponding spatio-temporal change of pore fluid pressure is the principle output used as an input for the RaS model (Fig. 2). The hydraulic response of the model to the stimulation operations at the borehole GPK4 of the Soultz-sous-Forêts reservoir in 2004 is shown in Fig. 3b. The pressure response of the model fits the general behaviour of the measured pressure. There is a discrepancy on the absolute level of overpressure measured at the wellhead (210 bar simulated vs. 170 bar measured), but bearing in mind that this was a forecast of the hydraulic response this discrepancy is of little importance. After less than about half a day an equilibrium pressure in GPK4 is reached; similarly, pressure reaches an equilibrium value away from the injection well quite fast, but on a lower pressure level. The non-linear pressure increases after increments of injection rate are matched very well.

The two RaS input parameters; i.e., the background shear stressing rate, $\dot{\tau}_r$, and the background seismicity rate, $r(x)$, are

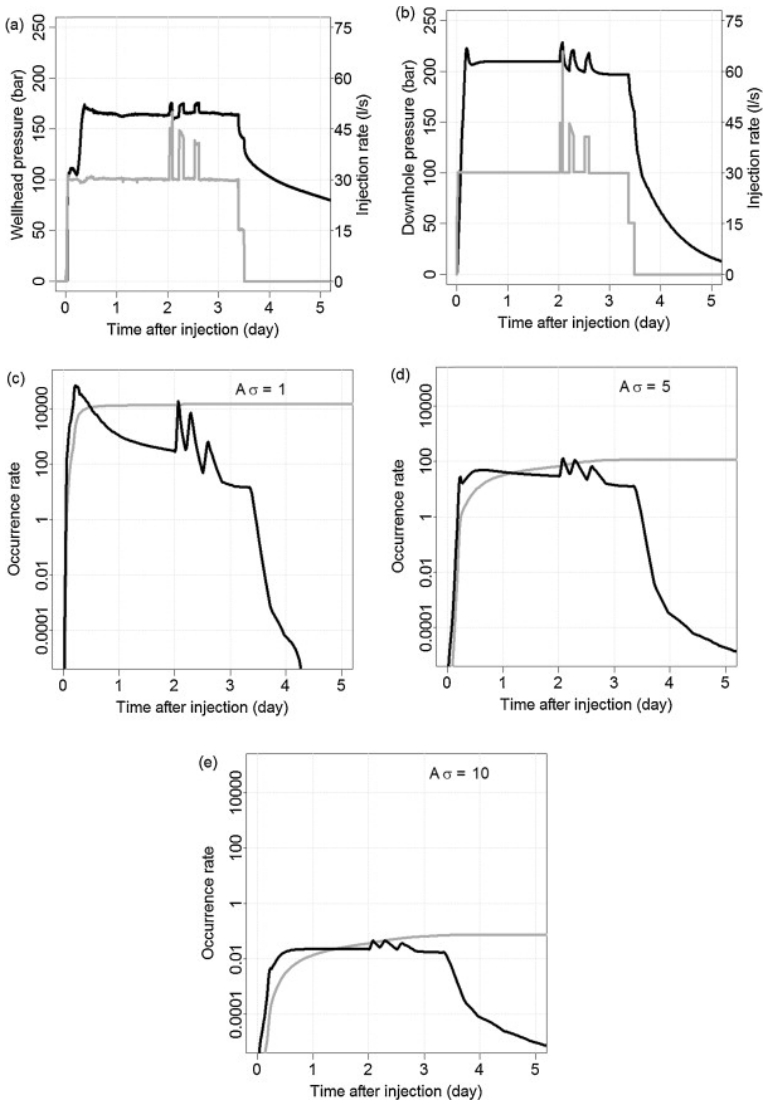


**Figure 3.** (a) Wellhead pressure (black curve) and injection rate (grey curve) for GPK4 well during the injection and after shut-in, (b) modelled downhole pressure (black curve) and injection rate (grey curve) for GPK4 well during the injection and after shut-in, (c) modelled seismicity rate (black curve) and cumulative seismicity rate (grey curve) using $A_\sigma$ = 1 bar, (d) $A_\sigma$ = 5 bar, (e) $A_\sigma$ = 10 bar.

selected using the seismicity parameters of the southern part of the Rhine Graben obtained by *Burkhard and Grünthal* (2009). The adopted $r(x)$ is derived based on the magnitude completeness of the induced seismicity catalogues from the GPK4 stimulation. For natural events with magnitudes $\geq 0.69$, the background seismicity rate is calculated as $r(x) = 10^{-7}$ events per day for each integration point in the reservoir. The background shear stress rate is arbitrarily considered as $\dot{\tau}_r = 10^{-7}$ bar per day, which is relatively low (compared to the stress changes caused by the reservoir activity), according to the fact that the calculated seismicity rate, $r(x)$, is low too.

From the numerical model, pore pressure changes are obtained for 1000 randomly located integration points and the RaS model is applied to each point to calculate the time-dependent seismicity rate. The integration points represent the locations of potential fractures in the reservoir. Finally, the induced seismicity rate in the whole reservoir is determined by integrating the seismicity rate over the 1000 integration points as described in Section 3. In Fig. 3c–e the seismicity rates and cumulative number of events are shown for three values of the parameter $A_\sigma$ of the RaS model.

The shape of the modelled seismicity rate changes strongly, when the parameter $A_\sigma$ changes from 1 to 10 bar (Fig. 3). As already mentioned above, the parameter $A_\sigma$ is the only free parameter in the RaS type models. It controls both the shape and the magnitude of the seismicity rate (*Dieterich*, 1994). For the application to tectonic processes, such as aftershock sequences, the parameter $A_\sigma$ is ranging between 0.05 and 1.0 bar (*Chan et al.*, 2010; *Harris and Simpson*, 1998; *Toda and Stein*, 2002; *Toda et al.*, 2002). The difference between $A_\sigma$ values in case of aftershock sequences, and the $A_\sigma$ values of 1–10 bar used here is substantial. A suitable value of $A_\sigma$ can be also selected by comparing the results of the modelled seismicity rate with the cumulative number of induced seismic events, if it is applicable. In our case only higher values of $A_\sigma$ shift the seismicity rates obtained from the RaS model into a reasonable level of induced seismicity rates (see Appendix). Furthermore, the physical processes involved during injection experiments are very different compared to tectonic earthquake interaction processes at greater depth on a pre-existing major fault. These are related to a single instantaneous major stress change followed by a stress relaxation process due to afterslip, visco-elastic relaxation of stresses and poro-elastic rebound (*Hergert and Heidbach*, 2006; *Masterlark and Hughes*, 2008). In contrast, the stress changes during stimulation experiments are not like sudden changes anymore, but they continuously change within time and thus they result in continuous changes in seismicity rate (*Häring et al.*, 2008). Moreover, during hydraulic stimulation mainly fractures are generated and thus it is to be expected that $A_\sigma$, which is represent-

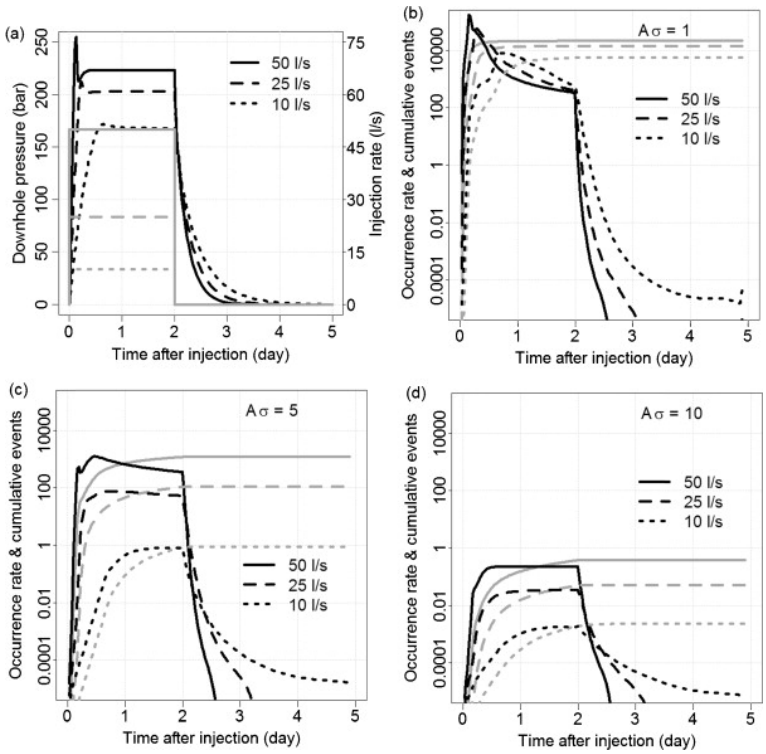


**Figure 4.** Constant injection scenarios: (a) modelled downhole pressure (black curve) and injection rate (grey curve) (b–d) modelled seismicity rate (black curve) and cumulative seismicity rate (grey curve) for $A_\sigma$ = 1 bar, $A_\sigma$ = 5 bar and $A_\sigma$ = 10 bar, respectively.

ing the physical fault behaviour, is different.

## 5. Synthetic injection scenarios

In order to test the effect of various injection strategies on the seismicity rate, our method is applied to three different synthetic injection scenarios. These scenarios are chosen such that they capture different injection strategies, which can be applied in field practice.

The first scenario is a constant injection for a duration of two days followed by the shut-in phase, which is captured by the geomechanical numerical model for another three days. We apply three different constant injection rates; i.e., 10, 25, and 50 L $s^{-1}$ (Fig. 4a). The purpose of this scenario is to analyse how the seismicity rate changes when applying different flow rates and pore pressures.

From Fig. 4 (and also from the later coming scenarios) it is evident that seismicity rate is exponentially proportional to the downhole pressure. This issue should be considered in real injection strategies. The soft stimulation realized by lower injection rates during longer stimulation time can cause the same value of cumulative seismicity as more intensive injection at higher flow rates, but needs a longer period of time to reach this value. If for example the 25 L $s^{-1}$ injection rate did not stop after two days but continued for a further about 20 days, then the corresponding cumulative seismicity could reach that of the 50 L $s^{-1}$ injection after two days. However, the slope of the cumulative seismicity rate curve is more gradual in the case of the soft injection. For real stimulation cases this means that operators will have more reaction time to control the seismicity; e.g., by reducing the injection rate.

In the next scenario we test a cyclic injection, where phases of constant injection rate are followed by shut-in. This cycle is repeated two more times and the injection rate is increased for each subsequent cycle, starting with 10 L $s^{-1}$ then 20 L $s^{-1}$ and finally 30 L $s^{-1}$ for the last cycle (Fig. 5a). We apply this scenario to analyse the effect of the re-injection on the induced seismicity rate.

From the cyclic injection scenario (Fig. 5), we see that, based on our approach, the effect of the fluid re-injection on the seismicity rate does not seem to be different from the effect of the injection itself.

In the last scenario we increase injection rate stepwise, starting at 10 L $s^{-1}$ for one day, then increases to 20 L $s^{-1}$ for another day and then increases again to 30 L $s^{-1}$. Shut-in is performed with stepwise decreasing injection rate to 20 L $s^{-1}$ and 10 L $s^{-1}$, respectively. Then, after a total time of five days the well is shut-in (Fig. 6a). The aim of applying this scenario is to study, how the seismicity rate changes with gradual changes of injection rate. The estimated seismicity rate for the stepwise injection scenario (Fig. 6) shows a gradual decrease, when the injection rate decreases step by step.

## 6. Discussion

So far, we introduced a prototype forward hybrid approach to estimate the induced seismicity rate caused by reservoir activities. This approach is based on two independent models, i.e., a geomechanical model to simulate the pore-pressure changes in the reservoir, and the RaS model to translate the pore-pressure changes in reservoir into the seismicity rate.

Mechanical modelling of a georeservoir is always a challenging task, which is related to the typically large uncertainties we have to deal with. The geomechanical numerical model used here relies on geological information obtained from well logs and the assumption of a homogeneous distribution of derived rock properties and stress field conditions in the reservoir. The initial hydraulic properties are of minor importance, as the geomechanical model converges to an equilibrium state given by the hydraulic loading conditions and the elastic and plastic enhancements of hydraulic conductivity. The adopted $b$-value must be chosen a priori based on earlier hydraulic experiments or historic seismicity. In the current framework, it is constant in time and space, although there are indications that this is not entirely valid for a hydraulic stimu-

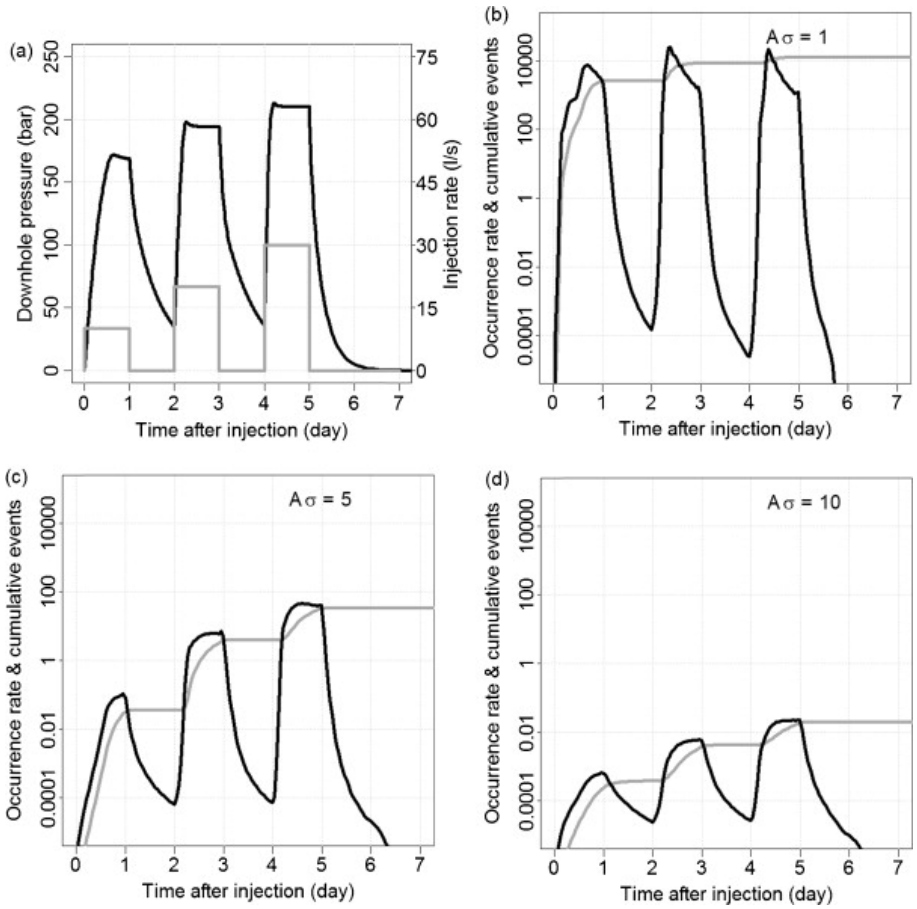


**Figure 5.** Cycling injection scenario: (a) modelled downhole pressure (black curve) and injection rate (grey curve) (b–d) modelled seismicity rate (black curve) and cumulative seismicity rate (grey curve) for $A_\sigma$ = 1 bar, $A_\sigma$ = 5 bar and $A_\sigma$ = 10 bar, respectively.

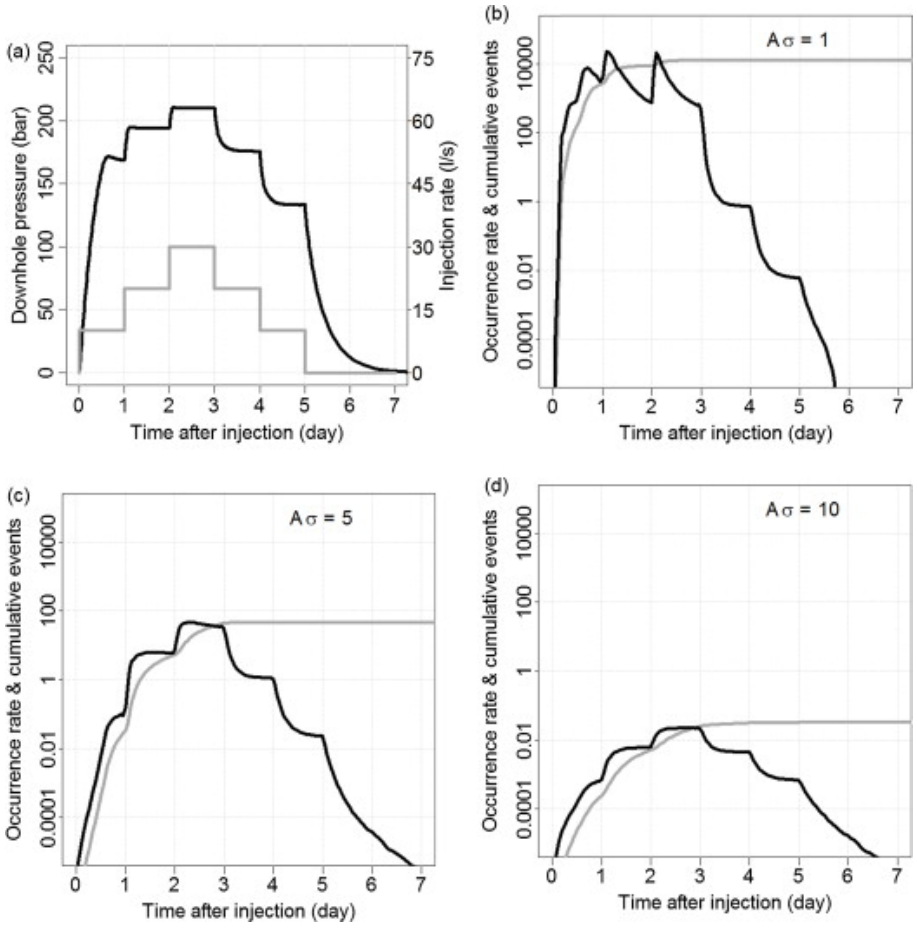


**Figure 6.** Stepwise injection scenario: (a) modelled downhole pressure (black curve) and injection rate (grey curve) (b–d) modelled seismicity rate (black curve) and cumulative seismicity rate (grey curve) for $A_\sigma$ = 1 bar, $A_\sigma$ = 5 bar and $A_\sigma$ = 10 bar, respectively.

lation scenario (*Bachmann et al.*, 2012). However, once an accepted model is found or put forward variations of the *b*-value are straightforward to implement.

The RaS model is a strong tool to translate the pore fluid stress into seismicity rate. $A_\sigma$ is the only free parameter of the RaS model. As already mentioned in Section 4, $A_\sigma$ can be either extracted from other reservoir studies, or adjusted using the cumulative number of induced events, if available. In general, changing parameter $A_\sigma$ results in a change in the seismicity rate. However, the qualitative behaviour of the seismicity rate does not explicitly change. This can be seen in Figs. 4–6 where logarithmic seismicity rates for the three scenarios with $A_\sigma$ = 1 bar, $A_\sigma$ = 5 bar and $A_\sigma$ = 10 bar, respectively, are shown. For relative smaller $A_\sigma$ = 1 bar corresponding to each subfigure (b) of Figs. 4–6, the seismicity rate is more sensitive to the changes of pore pressure than for larger $A_\sigma$. In contrast, for relative larger values of $A_\sigma$ = 10 bar corresponding to subfigures (d), the effect of the changes of pore pressure on the seismicity rate strongly decreases.

In order to calculate the potential probability of occurrence of induced events of a given magnitude class, the frequency–magnitude *b*-value is also required additional to the seismicity rate. The *b*-value can be either taken from other reservoir studies, or calculated by simulation of induced seismicity including magnitudes. The latter needs more assumptions, e.g. the size and geometry of predefined fractures as well as the magnitude of in situ stress. It should be also mentioned that the *b*-value in the case of induced seismicity is strongly time-dependent (*Bachmann et al.*, 2012) and different from *b*-values of the tectonic earthquakes (*Grünthal*, 2013). However, the focus of the RaS model applied in this study is the estimation of the seismicity rate but not the estimation of the *b*-value. In other words, the RaS model applied in this study does not simulate any event magnitude.

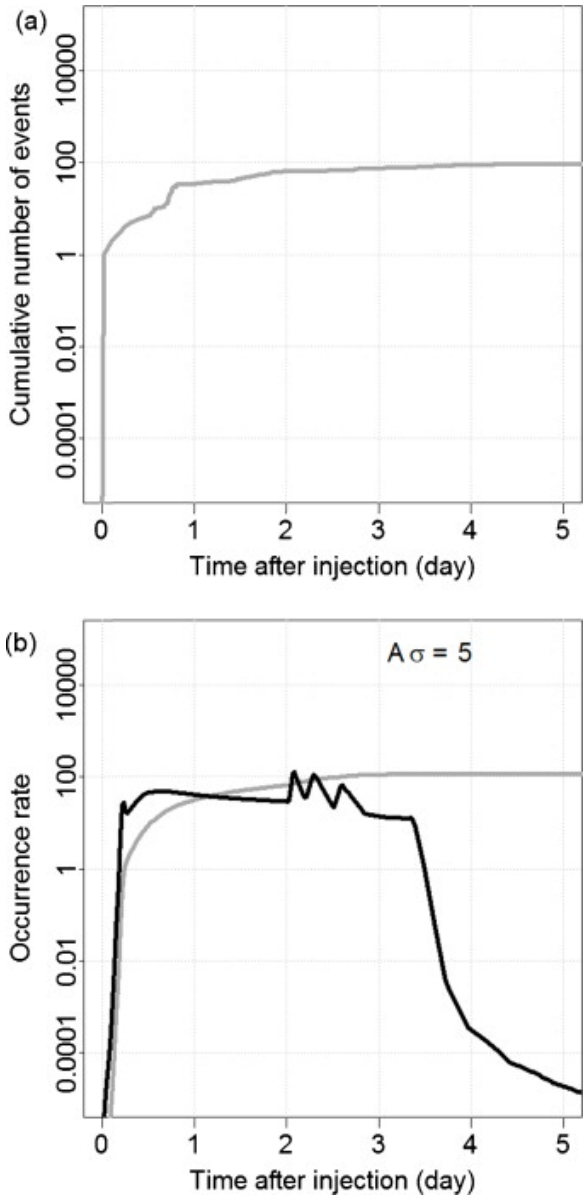


**Figure A.1.** (a) Cumulative number of the 96 induced events (logarithmic) beyond the magnitude completeness of $M_w \geq 0.69$, (b) modelled seismicity rate (black curve)and cumulative seismicity rate (grey curve) using $A_\sigma$ = 5 bar.

## 7. Conclusions

We introduced a new approach to translate the results of a geomechanical–numerical forward model in terms of stress changes into seismicity rate. This approach, in general, requires no induced seismicity data and can be used as a tool to pre-estimate the effect of man-made induced stress changes in the subsurface; e.g., due to fluid injection during stimulation experiments, shut-in of fluid injection or production of fluids, on the seismicity rate. The two input parameters; i.e., the background seismicity rate and the background stressing rate, can be estimated using available seismic hazard and stress information at the EGS area. The single free parameter of the RaS model, the $A_\sigma$, can be, either experimentally obtained, or estimated when seismicity data is available.

For our prototype model we apply a geomechanical numerical model and feed its output of change of effective stress into a time-dependent RaS model to estimate the seismicity rate induced by any stress changes in a georeservoir. In principle the hybrid modelling approach is able to predict seismicity arousing from stress changes caused by all kinds of sources, such as effects of poroelasticity (*Schoenball et al.*, 2010), temperature or chemical processes and couplings of these (*Bächler and Kohl*, 2005), as long as the underlying geomechanical numerical model is able to describe such mechanisms and translates it into changes of stress. The approach is applied to the Soultz-sous-Forêts geothermal site for the injection experiment in borehole GPK4 in 2004, using three different values of the parameter $A_\sigma$ (1, 5 and 10 bar) for the RaS model.

The strength of our approach is the capability to a priori test different injection scenarios, which we exemplify by constant injection, cyclic injection, and stepwise injection scenarios. The scenarios exhibit an explicit coupling between downhole pressure and seismicity rate. Seismicity can consequently be controlled by increase and decrease in the injection rate. Furthermore, the results of the synthetic injections show that a soft injection scenario can reproduce the same amount of events as a rapid injection scenario, but in a longer time span. This means in practice that there is longer reaction time, as seismicity progresses slower. In contrast, a sudden large increase in the injection rate can cause a large impulsive increase in the seismicity rate. This results in a large increase of the probability of occurrence of a larger magnitude event. We emphasize here that the hybrid approach can be used for any type of geomechanical reservoir model.

## Acknowledgements

The work presented was funded by the European Commission within the FP7 project GEISER, grant agreement no. 241321, by the Department of Energy Geothermal Technologies Programme under Award Number DE-EE0002756-002 and by EnBW Energie Baden-Württemberg AG. We thank

GEIE, Soultz and EOST, Strasbourg for providing data from the Soultz project and GEOWATT AG, Zürich for providing the Soultz model. We also thank Dietrich Stromeyer for discussion and improvement of the integration procedure. We acknowledge the valuable suggestions and comments in the frame of reviews from Nicholas Davatzes and another anonymous reviewer.

## Appendix A.

In order to adjust the free parameter $A$ of the RaS model, the results of the modelled seismicity rate are compared with the cumulative number of observed induced seismic events of the GPK4 injection experiment. In order to do this, we first estimate the magnitude completeness of the catalogue obtained from the surface monitoring network (*Dorbath et al.*, 2009) that contains 468 events. Using the method of *Wiemer and Wyss* (2000) to estimate the magnitude completeness we find that the catalogue is complete for the 96 events with $M_w \geq 0.69$. The cumulative number of events is shown in Fig. A.1a. The best fit to this curve of observed seismicity with the output of our hybrid model that translate stress changes from the geomechanical numerical model into seismicity rates is reached with $A_\sigma$ = 5 bar (Fig. A.1b). This understrikes the discussion in Section 4 of this paper that the $A_\sigma$ value for stimulation experiments is not to be expected in the range of $A_\sigma$ values from aftershock series of tectonic earthquakes.

## References

Altmann, J., Müller, T., Müller, B., Tingay, M., Heidbach, O., 2010. Poroelastic contribution to the reservoir stress path. International Journal of Rock Mechanics and Mining Sciences 47 (7), 1104–1113.

Bächler, D., Kohl, T., 2005. Coupled thermal–hydraulic–chemical modelling of enhanced geothermal systems. Geophysical Journal International 161 (2), 533–548.

Bachmann, C.E., Wiemer, S., Goertz-Allmann, B.P., Woessner, J., 2012. Influence of pore-pressure on the event-size distribution of induced earthquakes. Geophysical Research Letters 39 (9), 1–7, http://dx.doi.org/10.1029/2012GL051480.

Baisch, S., Voros, R., Rothert, E., Stang, H., Jung, R., Schellschmidt, R., 2010. A numerical model for fluid injection induced seismicity at Soultz-sous-Forêts. International Journal of Rock Mechanics and Mining Sciences 47 (3), 405–413.

Barth, A., Wenzel, F., Langenbruch, C., 2013. Probability of earthquake occurrence and magnitude estimation in the post shut-in phase of geothermal projects. Journal of Seismology 17 (1), 5–11.

Bommer, J.J., Oates, S., Cepeda, J.M., Lindholm, C., Bird, J., Torres, R., Marroquin, G., Rivas, J., 2006. Control of hazard due to seismicity induced by a hot fractured rock geothermal project. Engineering Geology 83, 287–306.

Bruel, D., 2007. Using the migration of induced seismicity as a constraint for fractured hot dry rock reservoir modelling. International Journal of Rock Mechanics and Mining Sciences 44, 1106–1117.

Burkhard, M., Grünthal, G., 2009. Seismic source zone characterization for the seismic hazard assessment project PEGASOS by the Expert Group 2 (EG1b). Swiss Journal of Geosciences 102, 149–188.

Catalli, F., Cocco, M., Console, R., Chiaraluce, L., 2008. Modeling seismicity rate changes during the 1997 Umbria-Marche sequence (central Italy) through a rate- and state-dependent model. Journal of Geophysical Research 113, B11301.

Chan, C.-H., Sørensen, M., Stromeyer, D., Grünthal, G., Heidbach, O., Hakimhashemi, A., Catalli, F., 2010. Forecasting Italian seismicity through a spatio-temporal physical model: importance of considering time-dependency and reliability of the forecast. Annals of Geophysics 53 (3), 129–140.

Cornell, C.A., 1968. Engineering seismic risk analysis. Bulletin of the Seismological Society of America 58, 1583–1606.

Daniel, G., Prono, E., Renard, F., Thouvenot, F., Hainzl, S., Marsan, D., Helmstetter, A., Traversa, P., Got, J.L., Jenatton, L., Guiguet, R., 2011. Changes in effective stress during the 2003–2004 Ubaye seismic swarm, France. Journal of Geophysical Research-Solid Earth 116, B01309.

Deichmann, N., Ernst, J., 2009. Earthquake focal mechanisms of the induced seismicity in 2006 and 2007 below Basel (Switzerland). Swiss Journal of Geosciences 102, 457–466.

Deichmann, N., Giardini, D., 2009. Earthquakes induced by the stimulation of an enhanced geothermal system below Basel (Switzerland). Seismological Research Letters 80 (5), 784–798.

Dieterich, J., 1994. A constitutive law for rate of earthquake production and its application to earthquake clustering. Journal of Geophysical Research 99 (B2), 2601–2618.

Dieterich, J., Cayol, V., Okubo, P., 2000. The use of earthquake rate changes as a stress meter at Kilauea volcano. Nature 408 (6811), 457–460.

Dinske, C., Shapiro, S., 2013. Seismotectonic state of reservoirs inferred from magnitude distributions of fluid-induced seismicity. Journal of Seismology 17 (1), 13–25.

Dorbath, L., Cuenot, N., Genter, A., Frogneux, M., 2009. Seismic response of the fractured and faulted granite of Soultz-sous-Forêts (France) to 5 km deep massive water injections. Geophysical Journal International 177 (2), 653–675.

Evans, K.F., Zappone, A., Kraft, T., Deichmann, N., Moia, F., 2012. A survey of the induced seismic response to fluid injection in geothermal and $CO_2$ reservoirs in Europe. Geothermics 41, 30–54.

Ghassemi, A., Zhou, X., 2011. A three-dimensional thermo-poroelastic model for fracture response to injection/extraction in enhanced geothermal systems. Geothermics 40 (1), 39–49.

Grünthal, G., 2013. Induced seismicity related to geothermal projects versus natural tectonic earthquakes and other types of induced seismic events in Central Europe. Geothermics http://dx.doi.org/10.1016/j.geothermics.2013.09.009

Grünthal, G., Wahlström, R., 2006. New generation of probabilistic seismic hazard assessment for the area Cologne/Aachen considering the uncertainties of the input data. Natural Hazards 38, 159–176.

Häring, M.O., Schanz, U., Ladner, F., Dyer, B.C., 2008. Characterisation of the Basel 1 enhanced geothermal system. Geothermics 37 (5), 469–495.

Harris, R., Simpson, R.W., 1998. Suppression of large earthquakes by stress shadows: a comparison of Coulomb and rate-and-state failure. Journal of Geophysical Research 103, 24439–24451.

Hergert, T., Heidbach, O., 2006. New insights in the mechanism of postseismic stress relaxation exemplified by the June 23rd 2001 $M_w$ = 8.4 earthquake in southern Peru. Geophysical Research Letters 33, L02307.

Hillis, R., 2000. Pore pressure/stress coupling and its implications for seismicity. Exploration Geophysics 31, 448–454.

Kohl, T., Evans, K.F., Hopkirk, R.J., Rybach, L., 1995. Coupled hydraulic, thermal and mechanical considerations for the simulation of hot dry rock reservoirs. International Journal of Rock Mechanics and Mining Sciences and Geomechanics Abstracts 33 (3), 130A–1130A.

Kohl, T., Evans, K.F., Hopkirk, R.J., Jung, R., Rybach, L., 1997. Observation and simulation of non-Darcian flow transients in fractured rock. Water Resources Research 33, 407–418.

Kohl, T., Mégel, T., 2007. Predictive modeling of reservoir response to hydraulic stimulations at the European EGS site Soultz-sous-Forets. International Journal of Rock Mechanics and Mining Sciences 44 (8), 1118–1131.

Majer, E., Nelson, J., Robertson-Tait, A., Savy, J., Wong, I., 2012. Protocol for addressing induced seismicity associated with enhanced geothermal systems. U.S. Department of Energy DOE/EE-0662.

Majer, E.L., Baria, R., Stark, M., Oates, S., Bommer, J., Smith, B., Asanuma, H., 2007. Induced seismicity associated with enhanced geothermal systems. Geothermics 36, 185–222.

Masterlark, T., Hughes, K.L.H., 2008. Next generation of deformation models for the 2004 M9 Sumatra-Andaman earthquake. Geophysical Research Letters 35, L19310.

McClure, M.W., Horne, H.N., 2011. Investigation of injection-induced seismicity using a coupled fluid flow and rate and state friction model. Geophysics 76 (6), WC183–WC200.

McGuire, R.K., 2004. Seismic Hazard and Risk Analysis. Earthquake Engineering Research Institute MNO-10, 240 p.

Passarelli, L., Maccaferri, F., Rivalta, E., Dahm, T., Abebe Boku, E., 2013. A probabilistic approach for the classification of earthquakes as 'triggered' or 'not triggered'. Journal of Seismology 17, 165–187.

Rutqvist, J., Birkholzer, J., Cappa, F., Tsang, C.-F., 2007. Estimating maximum sustainable injection pressure during geological sequestration of $CO_2$ using coupled fluid flow and geomechanical fault-slip analysis. Energy Conversion and Management 48, 1798–1807.

Schoenball, M., Müller, T.M., Müller, B., Heidbach, O., 2010. Fluid-induced micro-seismicity in pre-stressed rock masses. Geophysical Journal International 180, 113–119.

Shapiro, S.A., Dinske, C., Langenbruch, C., Wenzel, F., 2010. Seismogenic index and magnitude probability of earthquakes induced during reservoir fluid stimulations. The Leading Edge, 304–309.

Shen, B., Kim, H.-M., Park, E.-S., Kim, T.-K., Wuttke, M.W., Rinne, M., Backers, T., Stephansson, O., 2013. Multi-region boundary element analysis for coupled thermal-fracturing processes in geomaterials. Rock Mechanics and Rock Engineering 46, 135–151.

Suckale, J., 2009. Induced seismicity in hydrocarbon fields. Advances in Geophysics 51, 55–106.

Suckale, J., 2010. Moderate-to-large seismicity induced hydrocarbon production. The Leading Edge 29, 310–317.

Tester, J.W., Anderson, B.J., Batchelor, A.S., Blackwell, D.D., DiPippo, R., Drake, E.M., Garnish, J.D., Livesay, B., Moore, M.C., Nochols, K., Petty, S., Toksoez, M.N., Veatch, R.W.J., 2006. The Future of Geothermal Energy: Impact of Enhanced Geothermal Systems (EGS) on the United States in the 21st Century. MIT Report. Massachusetts Institute of Technology, 372 pp., Available at: http://www1.eere.energy.gov/geothermal/pdfs/future_geo_energy.pdf (last accessed 04.11.13).

Toda, S., Stein, R., 2003. Toggling of seismicity by the 1997 Kagoshima earthquake couplet: a demonstration of time-dependent stress transfer. Journal of Geophysical Research 108 (B12).

Toda, S., Stein, R.S., Sagiya, T., 2002. Evidence from the AD 2000 Izu islands earthquake swarm that stressing rate governs seismicity. Nature 419 (6902), 58–61.

Toda, S., Stein, R.S., 2002. Response of the San Andreas fault to the 1983 Coalinga-Nunez earthquakes: an application of interaction-based probabilities for Parkfield. Journal of Geophysical Research, 107.

Wiemer, S., Wyss, M., 2000. Minimum magnitude of complete reporting in earthquake catalogs: examples from Alaska, the western United States, and Japan. Bulletin of Seismological Society of America 90, 859–869.

Willis-Richards, J., Watanabe, K., Takahashi, H., 1996. Progress toward a stochastic rock mechanics model of engineered geothermal systems. Journal of Geophysical Research-Solid Earth 101 (B8), 17481–17496.

Yoon, J.S., Zang, A., Stephansson, O., 2012. Simulating fracture and friction of Aue granite under confined asymmetric compressive test using clumped particle model. International Journal of Rock Mechanics and Mining Sciences 49, 68–83.

Yoon, J.S., Zang, A., Stephansson, O., 2013. Hydro-Mechanical Coupled Discrete Element Modeling of Geothermal Reservoir Stimulation and Induced Seismicity. In: Hou, M.Z., et al. (Eds.), Clean Energy Systems in the Subsurface. SSGG, pp. 221–231.